High-repetition-rate femtosecond optical parametric oscillator–amplifier system near 3 μm

Gary R. Holtom, Robert A. Crowell, and X. Sunney Xie

Environmental Molecular Sciences Laboratory, Pacific Northwest Laboratory, P.O. Box 999 Mail Stop K2-14, Richland, Washington 99352

Received October 17, 1994; revised manuscript received May 9, 1995

An ultrafast laser system for the chemically important 3-μm spectral region has been constructed by means of noncritically phased-matched $KTiOPO_4$ optical parametric gain elements. An optical parametric oscillator, synchronously pumped by a mode-locked Ti:sapphire oscillator, generates high-quality seed pulses for an optical parametric amplifier. The optical parametric amplifier, pumped by a high-repetition-rate Ti:sapphire regenerative amplifier, amplifies the seed pulses by a factor of 520. Pulses with an energy of 550 nJ and a pulse width of 160 fs are produced at a 250-kHz repetition rate in the 3-μm region.

1. INTRODUCTION

Infrared spectroscopy in the 3-μm region provides a wealth of structural information on chemical and biological systems. The fundamental stretching modes for the -OH_x, -CH_x, and -NH_x groups lie in this important spectroscopic region. For example, water, the most common solvent, has a very broad OH infrared absorption band near the 3-μm region. Picosecond hole-burning experiments in this spectral region have suggested that such a broad band is inhomogeneously broadened because of distinctly different hydrogen-bonded structures.[1] The sensitivity of the water OH-stretching frequencies to the hydrogen-bond environment suggests that time-resolved infrared spectroscopic studies of this band should provide useful information about the structure and the dynamics of the water hydrogen-bond network. However, the inhomogeneous nature of this infrared band requires the implementation of time-resolved nonlinear coherent methods, such as infrared photon echoes,[2,3] which require the use of high-peak-power femtosecond lasers. Femtosecond infrared spectroscopic measurements have not been made on water because of the lack of a suitable laser source in this spectral region. In this paper we describe an optical parametric oscillator–amplifier (OPO–OPA) system that provides 160-fs 550-nJ pulses in the 3-μm region at a 250-kHz repetition rate.

Recent advances in nonlinear optical materials, along with the advent of the mode-locked Ti:sapphire laser, have been followed closely by significant progress in the development of all-solid-state tunable laser sources by such methods as optical parametric generation,[4–7] optical parametric amplification,[4–12] and optical parametric oscillation.[5,11,13–30] However, most of the research in this area has focused on the visible and the near-infrared spectral regions. Development of high-repetition-rate, high-peak-power, femtosecond laser sources in the chemically important mid-infrared region is still lacking. OPO's synchronously pumped by mode-locked Ti:sapphire lasers have been shown to offer great convenience when a widely tunable source is required.[15–22] The crystals that are most commonly used in OPO's, β-BaB_2O_4,[6,10,12,31] and LiB_3O_5,[6,7,10,11,24,26,29] have increasing absorption losses at wavelengths longer than approximately 2.5 μm. Instead, we chose $KTiOPO_4$ (KTP) and its isomorphs, which are transparent and tunable in the 3-μm region.[4,15,25,28,32]

Although synchronously pumped OPO's do offer the advantage of high repetition rates (70–80 MHz) and broad tunability, the pulse energy produced ($\leq$4 nJ) is low. To perform nonlinear spectroscopic measurements, an OPA is necessary. As is shown in this paper, the output of the OPO can be used to seed an OPA, resulting in pulse-energy amplification factors as high as 520. Generating femtosecond infrared pulses with an OPO-seeded OPA offers distinct advantages over seeding with an optical parametric generator[4,6,11] or difference-frequency mixing.[11] Because it is possible to generate high-quality (i.e., transform-limited, TEM_{00}) seed pulses in an OPO, the conversion efficiencies in the OPA are much higher for OPO seeding (30–35%) when compared with seeding by optical parametric generation (typically 10–15%). This increase in efficiency permits the use of lower-energy pump sources, which in turn permits the use of higher-repetition-rate pump lasers for the OPO-seeded OPA.

In this paper we demonstrate a high-repetition-rate (250-kHz), high-peak-power ($\geq$3 MW), femtosecond OPO–OPA system designed to conduct time-resolved nonlinear spectroscopic measurements in the 3-μm spectral region. The system is based on a noncritically phased-matched KTP OPO that is synchronously pumped by a Ti:sapphire laser.[14,30,33] The signal wave from the OPO is used to seed a noncritically phased-matched KTP OPA that is pumped by a 250-kHz Ti:sapphire regenerative amplifier. The idler wave (2.75 μm) from the OPA consists of 160-fs pulses with energies of 550 nJ. Tuning of the idler wave in the range of 2.5–2.9 μm is achieved by tuning of the Ti:sapphire pump laser. This tuning range in the system is limited by the reflectivity range of the mirrors in the OPO and by the pulse-compression optics in the regenerative amplifier. Tuning beyond 3.2 μm is not practical in this system because of the onset of a strong infrared absorption in KTP at this wavelength.

0740-3224/95/091723-09$06.00

Recently we showed that this system has sufficient time resolution (≤100 fs) to permit measurement of the dephasing dynamics of liquid-water molecules at room temperature.[34,35]

Other methods that can be used to generate ultrashort pulses in the mid-infrared spectral region include the free electron laser,[2,3] color-center lasers,[36] and difference-frequency mixing.[4,11,37] The OPO–OPA system offers distinct advantages over these methods for generating high-repetition-rate, high-peak power femtosecond pulses in this wavelength region. Free electron lasers have been shown to be capable of performing nonlinear spectroscopic measurements in the mid-infrared region.[2,3] However, for measurements with hydrogen-bonded liquids, a subpicosecond time resolution is required.[34,35] Additionally, free electron lasers require a large accelerator facility, which limits their availability. Color-center lasers provide a tunable source in the mid-infrared region. However, the pulse widths are near 10 ps, which again is too broad to measure liquid-water vibrational dynamics. Additionally, color-center lasers do not have sufficient pulse energy to permit performance of nonlinear experiments, and they tend to suffer from such problems as photobleaching, which makes them an unreliable source.[36] Finally, difference-frequency mixing is capable of generating short pulses with sufficient energy in the mid-infrared region.[4,37] But the high laser energies that are necessary to obtain a useful amount of infrared light require low-repetition-rate amplifiers (≤1 kHz) for the mixing pulses. As is shown below, the OPO–OPA combination offers superior conversion efficiencies when compared with those obtained from difference-frequency mixing.

2. CRYSTAL PROPERTIES

With KTP there are two possible phase-matching conditions that are capable of tuning the idler wave out to the water-absorption region (3 μm): type-II phase matching ($o \rightarrow e + o$) and type-III noncritical phase matching ($o \rightarrow o + e$). In a type-II OPO tuning is achieved through changing of the angle of the KTP crystal, whereas noncritical type-III OPO's must be tuned by changing of the wavelength of the pump laser. Type-II KTP OPO's were shown to be tunable in the 1.8–2.5-μm (idler-wave) and the 1.2–1.4-μm (signal-wave) spectral regions.[15,21,25,28,38] In general, a type-II OPO will have a much broader tuning range than a type-III noncritically phase-matched OPO. However, type-III noncritical phase matching has distinct advantages that make this type of phase matching preferable to type-II phase matching for KTP in the 3-μm region. The latter suffers from the following two difficulties as the signal and the idler waves are tuned far from degeneracy. First, operation with the idler wavelength in the region of 3 μm rather than in the previously reported[15,18,21] 2-μm region requires a decrease in θ from 48° to 41° [Fig. 1(A)]. The effective nonlinear coefficients (d_{eff}) decrease as θ decreases, as shown in Fig. 1(B). Second, at 41° the walkoff angle between the pump and the signal beams is approximately 3° internal to the crystal [Fig. 1(C)].[39] The momentum conservation requirement requires the angle between the pump- and the idler-wave vectors to become even larger than the angle between the pump and the signal waves, which results in low gain and extremely difficult alignment because of the increased difficulty in achieving the required beam overlap.[21,22]

These problems are avoided with type-III noncritical phase matching. The members of the KTP family of crystals are biaxial and have two noncritically phase-matched angles ($\theta = 90°$, $\phi = 0°$ and $\theta = 90°$, $\phi = 90°$).[40,41] We use the angle with the larger nonlinear coefficient, $\theta = 90°$ and $\phi = 0°$, which was reported previously.[14,30,33] The characteristics of type-II and type-III noncritical phase-matched operation are compared in Fig. 1. Two crystal angles, 42° and 90°, are phase matched to generate 2.7 μm. With respect to each curve shown in Fig. 1(A), the region to the left of the degeneracy point describes

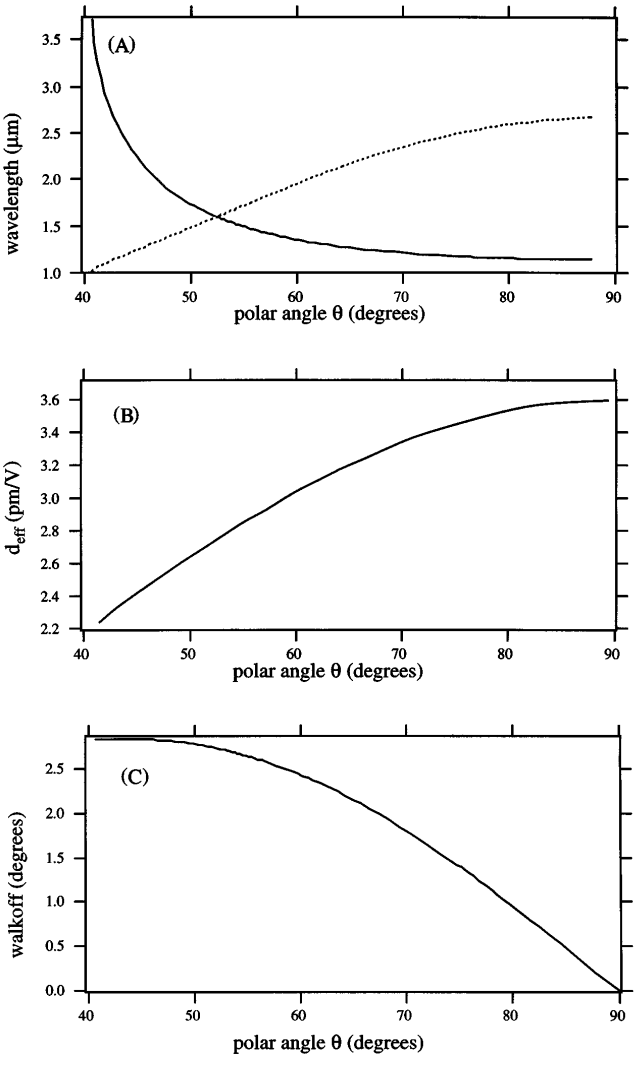

Fig. 1. (A) Tuning curve for type-II and type-III phase matching in KTP for 800-nm pumping. With respect to each curve, the region to the left of the degeneracy point (crossing point) corresponds to type-II phase-matching conditions, whereas the region to the right of the degeneracy point corresponds to type-III phase matching. The solid curve is an ordinary-type ray, and the dotted curve is an extraordinary-type ray. (B) d_{eff} as a function of θ. d_{eff} is at its maximum for noncritical phase matching ($\theta = 90°$). (C) Beam walkoff of the extraordinary-type ray as a function of θ. Note that the walkoff goes to zero at the noncritical-phase-matching angle.

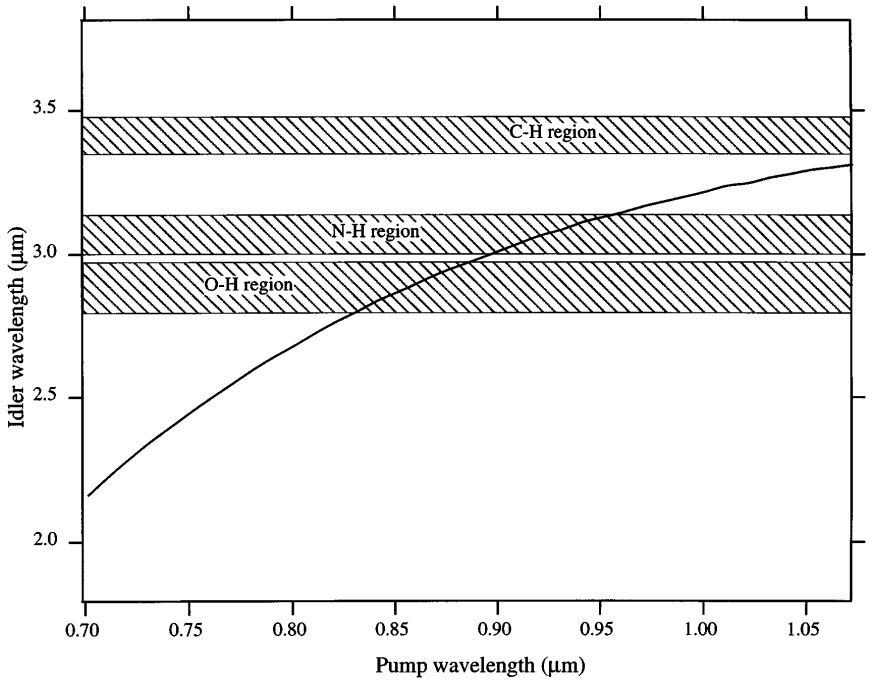

Fig. 2. Tuning curve for a noncritically phase-matched ($\theta = 90°$) KTP OPO and some of the chemically important infrared absorption band found in this region. The OPO–OPA system reported here is tunable in the 2.5–2.9-μm range, with pump wavelengths of 760–880 nm.

type-II phase matching, and that to the right of the degeneracy point describes type-III phase matching, for which the pump and the signal waves are of the ordinary type.

Figure 1(C) shows the calculated walkoff of the signal and the idler waves. The pump wave propagates as an ordinary-type ray. For noncritical phase matching the walkoff goes to zero at $\theta = 90°$. Because of zero walkoff for type-III noncritical phase matching, all three waves (the pump, the signal, and the idler) propagate collinearly, which greatly simplifies cavity alignment. The disadvantage of type-III phase matching is that tuning the idler wavelength requires changing the pump wavelength. Variants of KTP, namely, $RbTiOAsO_4$,[22] $CsTiOAsO_4$,[16] and $KTiOAsO_4$,[17] also permit noncritical phase-matched OPO operation over most of the region from 1.1 to 3.1 μm, with pump wavelengths near the gain maximum of the Ti:sapphire laser. We chose the most birefringent crystal, KTP, because it provides the longest idler wavelength at convenient pump wavelengths. Figure 2 shows the calculated tuning curve for the system, along with the chemically important infrared bands that are found in this spectroscopic region. The tuning curve shown in Fig. 2 is calculated with the Sellmeier coefficients given in Ref. 42.

Finding the crystal length and the focusing conditions that maximize the gain while maintaining the desired pulse width requires a series of calculations.[43] We use the following strategy. For a given crystal, pulse width, and wavelength, walkoff is determined from Sellmeier equations describing the optical properties of the crystal.[39] The dispersion is also calculated, and a limiting crystal thickness is determined. For a given walkoff and a given crystal thickness a search is made for the optimal focal sizes by means of an analytical form for the overall gain.[43] Should the spot size for the signal wave be smaller than the cavity can support, the small-signal gain is recalculated for a spot size determined from the paraxial-ray analysis of the cavity.[44] The results for type-II and type-III noncritical phase matching are tabulated in Table 1. In general, when walkoff is present (type II), gain is optimized when the beams are

Table 1. Comparison of OPO Design Parameters for Angle-Tuned and for Noncritically Phase-Matched Operation in KTP, Calculated for 80-fs pump pulses

Parameter	OPO Design: Angle Tuned	OPO Design: Noncritically Phase Matched
Angle from z axis (deg)	42.5	90
Walkoff angle between pump and signal waves (deg; internal)	2.8	0
Relative nonlinear coefficient d_{eff} (pm/V)	2.3	3.59
Optimal thickness of crystal (mm)	0.76	0.29
Optimal pump radius (μm)	7.8	2.5
Optimal signal radius (μm)	8.0	3.0
Calculated gain for 20-nJ pump pulses, optimal focus	0.38	1.8
Calculated gain for 20-nJ pump pulses with 21.5-μm signal and 15.5-μm pump radius	0.17	0.22

not focused as tightly as for the collinear case (type III, noncritical).

The experimental wavelengths are in excellent agreement with values calculated for type-III noncritical phase matching. Gains were estimated assuming a peak power of 250 kW from the pump laser. In both cases the pump wave is polarized perpendicular to the z axis. The signal wave is polarized parallel to the z axis for angle tuning, whereas the pump- and the signal-wave polarizations are the same for noncritical phase matching. In both cases the crystal thickness is limited by the difference in group velocity of the signal and the idler waves.[30]

Because of the greater dispersion of KTP at $\theta = 90°$, for noncritical phase matching a thinner crystal is required than for angle tuning. The pump, the signal, and the idler beams have the same optimum confocal parameter of approximately one third the crystal thickness, as shown in Ref. 45. This result is altered by the presence of walkoff, in which case the model predicts maximum gain when the three beams are more nearly the same size. Even with a thinner crystal at $\theta = 90°$, the gain is higher because of the very small spot sizes made possible by the large acceptance angle, the absence of walkoff, and the higher nonlinear coefficient. The calculated optimal radius at the waist for angle tuning, 8 μm, is small but realizable in a practical cavity arrangement. Achieving the much smaller spot size of 3 μm for noncritical phase matching is not practical in an OPO cavity 2 m long. In this study larger spots (20-μm radius) for the signal wave were used, resulting in reduced gain. Obtaining smaller spots requires either a shorter radius of curvature for the focusing mirrors or a less stable cavity. However, even for the large spot size, the gain is sufficient for convenient operation of the OPO and is higher than previously reported.[14,30]

3. TI:SAPPHIRE PUMP LASERS

The major components of the OPO–OPA system are combined to form the overall system as shown in Fig. 3. The reported powers are approximately 95% of the best-ever powers, a point at which they operate routinely.

The Ti:sapphire laser (Coherent Mira Basic) and the regenerative amplifier (Coherent Rega) are simultaneously pumped with 12.7 and 15.5 W, respectively, from a multiline argon-ion laser (Coherent Innova 425). We modified the Ti:sapphire laser by replacing the SF-10 (Schott) prisms with lower-dispersion LaF-26 prisms (Schott), adding a thermal compensation device to stabilize the cavity length, and using a low-dispersion birefringent tuning element (Coherent). The Ti:sapphire laser is operated at a pulse width of 115 fs at a wavelength of 816 nm. The pulses from the Ti:sapphire laser are chirped and are compressed to a pulse width of 85 fs with a pair of SF-11 (Schott) prisms in double-pass configuration external to the laser cavity. The spectrum is nearly symmetric, with a full width at half-maximum (FWHM) of 12.6 nm. Assuming a sech^2 pulse shape results in a time–bandwidth product of 0.378, which is 1.2 times the transform limit. Typical output power is 1.95 W at a repetition rate of 76 MHz. Of this power approximately 200 mW is used for diagnostics and for seeding the regenerative amplifier, and the remaining 1.75 W is used for synchronous pumping of the OPO.

The high-energy pump pulses for the OPA are produced in a 250-kHz Ti:sapphire regenerative amplifier (Coherent Rega). The regenerative amplifier was modified in a manner similar to that described in Ref. 46. After compression the pulse energy is 6 μJ (1.5-W average power), with a pulse width of 90 fs (assuming a sech^2 pulse shape). The pulses coming out of the regenerative amplifier are 1.2 times the transform limit, assuming a sech^2 pulse shape.

4. OPTICAL PARAMETRIC OSCILLATOR

Although noncritically phase-matched KTP OPO's were previously demonstrated,[14,23,30,32] our system was optimized for operation in the 3-μm spectral region. The four-mirror OPO cavity (Fig. 4) is linear, with a C fold, and contains a pair of SF-10 prisms for dispersion compensation. The KTP crystals (Airtron) used in the OPO and the OPA are cut for the type-III noncritical-phase-matching condition ($\theta = 90°$, $\phi = 0°$) and are 0.9 mm thick, with a single-layer MgF_2 coating optimized for a minimum reflectivity at 1.06 μm. The crystals are hydrothermally grown and are selected for their resistance to gray (or dark) tracking. We observed no signs of gray tracking in these crystals. Despite the high intensity of the focused pump laser (approximately 5×10^{10} W/cm^2) and the even larger in-cavity power of the signal wave (as much as an order of magnitude higher), optical damage is not observed.

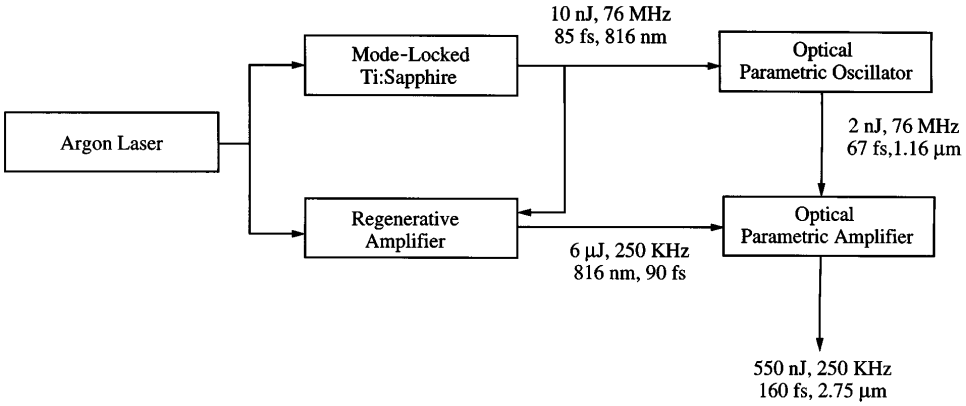

Fig. 3. Block diagram showing the overall OPO–OPA system design.

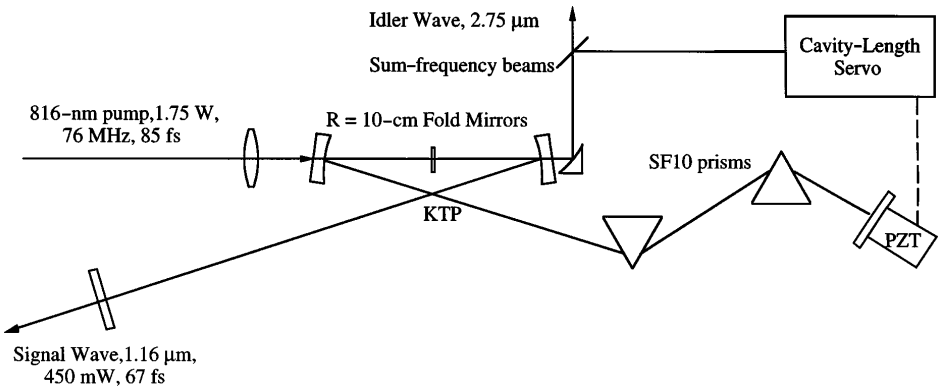

Fig. 4. Schematic diagram of the noncritically phase-matched KTP OPO.

The KTP crystal is centered between two 10-cm radius-of-curvature folding mirrors. The pump and the signal beams are polarized horizontally and propagate along the x axis of the crystal. The idler wave is polarized vertically (parallel to the z axis). All three beams, the pump, the signal, and the idler, propagate collinearly. At a pump wavelength of 816 nm the signal and the idler wavelengths of the OPO are 1.16 and 2.75 μm, respectively. The idler beam can be extracted from the cavity from one of the fold mirrors, which is made from a sapphire substrate. However, the reflective coating on this optic absorbs approximately 70% of the idler beam at 2.75 μm.

Cavity alignment is performed by a method similar to the one described in Ref. 30. Briefly, the KTP crystal is replaced with a 1-mm-thick Nd:YAG slab. All cavity adjustments can be optimized by maximization of the power out of the Ti:sapphire-pumped Nd:YAG laser. The cavity length can be determined to within a few parts per million by measurement of the beat frequency of the longitudinal modes. Lasing is then easily achieved by replacement of the Nd:YAG crystal with the KTP crystal, followed by fine adjustment of the cavity length.

Small deviations in the cavity length result in synchronous pumping efficiencies that are less than ideal and in substantial fluctuations in the pulse spectrum. Translation of an end mirror by a distance of 3 μm is sufficient to stop the lasing. For long-term stability it becomes essential to use active cavity-length stabilization to keep the OPO synchronized with the Ti:sapphire pump laser. Small changes in the OPO cavity length result in measurable spectral shifts in the signal wave, which provide an error signal for a servo loop.[38] A grating is used to disperse the small amount of signal wave (leaking out of the sapphire fold mirror) across a pair of germanium photodiodes. The difference output from the photodiodes is used as a feedback signal to drive a piezoelectric tube that is mounted to one of the cavity end mirrors. By keeping the spectrum of the signal wave constant the OPO is kept synchronous with the pump laser. Ambient acoustic noise, air currents, and any contact with a mirror mount cause cavity-length changes by a substantial fraction of a micrometer. By setting the OPO on a super-Invar breadboard and using a passive thermal compensator in the Ti:sapphire oscillator, the long-term drift is kept within a few micrometers over the course of a working day.

As previously reported,[14] synchronously pumped OPO's can operate with either positive or negative total cavity dispersion. In the near-zero and the positive-dispersion regimes the signal wave of the OPO exhibits two large peaks in its spectrum, which makes it impossible to obtain transform-limited pulses. To obtain high-quality pulses, which are near the transform limit, it is necessary to operate the OPO in the negative-dispersion regime. In this case the OPO displays nearly transform-limited pulses at the expense of a 10% reduction in output power. Figure 5 shows the autocorrelation and the spectrum of the signal wave when the OPO is operated with slight negative dispersion. The autocorrelation width is 67 fs (assuming a sech^2 pulse shape), and the FWHM is 24.5 nm; these values give a time–bandwidth product of 0.378. The signal pulses are 1.2 times the transform limit for a sech^2 pulse, which is the same as the pump pulses.

We perform gain measurements by pumping the OPO at 1.8-W average power and measuring the signal-wave output power for output couplers with different amounts of transmission. The output power for a series of output couplers is plotted in Fig. 6. Following the recipe of Cheung and Liu,[43] we choose the 90% reflectivity so that the OPO operates at twice threshold power. This percentage is nearly optimal for both conversion efficiency and pulse width. The measured gain of a little more than 20% is close to the value of 25% calculated from analytical models based on a 20-μm signal-beam radius. This result is significantly greater than those previously reported.[14,23,30,32] Power available during routine operation is 450 mW in the signal wave (by means of a 10% output coupler), with a stability comparable with that of the pump laser. Substantial power of more than 100 mW is available in the idler wave, depending on the absorption of the idler in the output mirror.

A useful measure of the efficiency of the OPO can be determined from the depletion of the pump laser, which is 55% with the 10% output coupler. Our measured output powers with different output couplers can be rationalized by a total round-trip linear loss of approximately 4% in addition to the output coupling. A round-trip loss of approximately 2% is expected from the antireflection coatings on the KTP crystal because our operating wavelength is longer than the design wavelength for the coating.

Several additional visible wavelengths are produced in the OPO because of nonresonant frequency mixing of the collinear beams. These are the second harmonic of

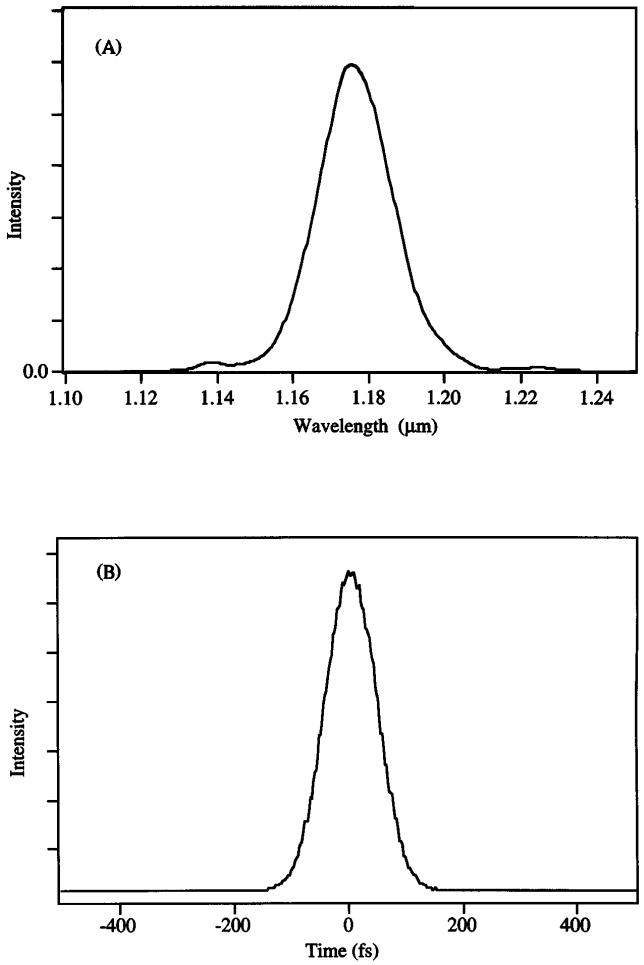

Fig. 5. (A) Spectrum of the OPO signal wave with a pump wavelength of 817 nm. The FWHM is 24.5 nm. (B) Autocorrelation of the signal wave out of the OPO. The FWHM is 67 fs, assuming a sech^2 pulse shape. The pulses in the signal branch of the OPO are 1.2 times the transform limit.

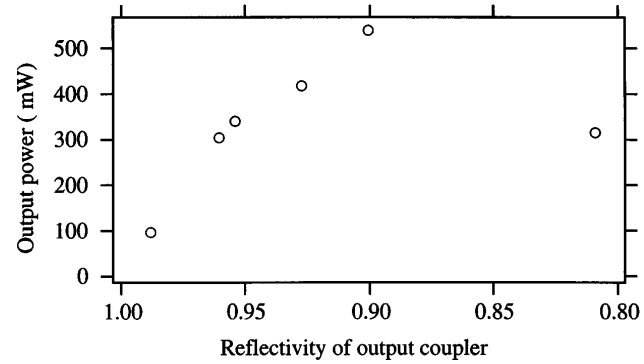

Fig. 6. Signal output power as a function of the reflectivity of the output coupler for the KTP OPO.

the signal (582 nm), the sum of the pump and the idler (630 nm), the sum of the pump and the signal (480 nm), and the second harmonic of the pump (408 nm). They are produced at fractional milliwatt levels and leak out of the cavity at various mirrors. The 582-nm beam is generated in both directions, and, because it is strictly collinear with the signal wave, it becomes a particularly useful tool for alignment of the delay-line connecting the OPO to the OPA. When dispersed, this beam gives a convenient estimate of the spectral width (inverse pulse width) of the signal wave.

5. OPTICAL PARAMETRIC AMPLIFIER

A schematic diagram of the OPA is shown in Fig. 7. The pump pulses from the Ti:sapphire regenerative-amplifier pulses are brought in collinear with the signal wave from the OPO and are focused with an achromatic lens of 15-cm focal length into a KTP crystal identical to that used in the OPO. The energy of the 1.16-μm seed pulses is attenuated to energies of 2–2.5 nJ at the KTP crystal. The signal wave from the OPO is passed through a delay line so that it is temporally overlapped with the pump pulses. An enhanced silver-coated spherical mirror is used to reflect the three widely different wavelengths through the KTP crystal for a second pass (Fig. 7). The measured average power after a double pass in the OPA is 137 mW (550 nJ/pulse) in the idler wave. We did not measure the properties of the signal wave out of the OPA, but on the basis of the principle of conservation of energy it must have a pulse energy of at least 1.3 μJ.

Amplitude fluctuations in the regenerative-amplifier pulses are less than 1% peak to peak. The output from the OPA has a 1% peak-to-peak fluctuation. Over a longer period of time ($\geq$0.5 s) the OPA shows sudden

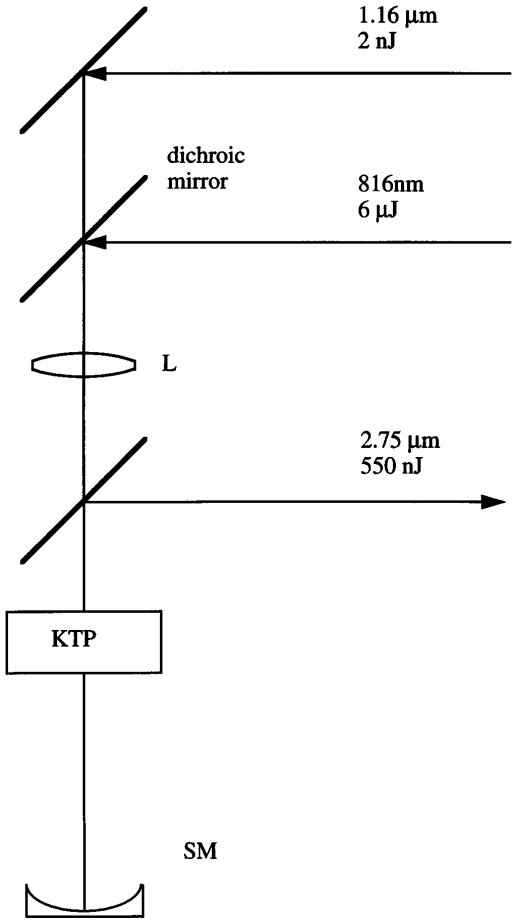

Fig. 7. Schematic of the noncritically phase-matched KTP OPA. L, 15-cm achromatic lens; SM, enhanced silver-coated 25-cm spherical mirror.

jumps in intensity (as high as 5%). The sudden intensity fluctuations in the OPA appear to be a result of air currents.

Long-term drift in the time correlation between the seed pulses from the OPO and the pump pulses requires a delay-line adjustment of the order of 2–3 mm over a period of 8 h. We attribute this effect to changes in the temperature of the regenerative-amplifier baseplate, which results in a substantial change in optical path length when amplified by the 20 or so round trips that the pulse makes in the cavity before ejection. Pulse overlap between the OPO seed pulse and the high-energy pump pulse is continuously optimized with a simple servo system. The OPO delay line is mounted on a motorized micrometer–piezoelectric-tube combination. The piezoelectric tube is used to dither (50 Hz) the delay line and the resulting modulations in the 630-nm output (nonphase-matched sum-frequency generation of the idler and the pump waves) of the OPA, which are monitored with a photodiode. The output of the photodiode is the input of a simple servo system that continuously adjusts the motorized micrometer to maximize the intensity at 630 nm. The OPA output remains stable over a period of several hours.

Most of the 550 nJ of pulse energy is attainable with only a single-pass OPA; however, this attainment requires tight focusing that results in severe degradation in the beam quality of the OPA output because of self-focusing in the KTP crystal. In addition to self-focusing, optical parametric generation and hyper-Raman scattering are observed in the OPA crystal under tight focusing conditions (power densities greater than $\sim$200 GW/cm^2). Obtaining an undistorted beam from the OPA while retaining good amplification requires defocusing of the pump beam and the addition of a second pass to the OPA. The empirical approach for optimizing the OPA is, for each pass, to focus as tightly as possible without producing self-focusing in the KTP. When self-focusing occurs, a striated pattern of red and green light appears, which is insensitive to the presence of a seed pulse from the OPO. By defocusing, the competing nonlinear processes are eliminated, with the exception of the 630-nm sum-frequency mixing beam of the idler and the pump and a of much weaker 480-nm beam from the signal and the pump sum-frequency generation. Defocusing by movement of the crystal away from the focus reduces the power to approximately 12 mW (50 nJ) in the first pass and results in a high-quality beam. The full output power is recovered in the second pass. An enhanced silver-coated mirror (Virgo) that has a reasonably high reflectivity at the three wavelengths ($\geq$97%) is used for refocusing. Figure 8 shows the autocorrelation and the spectrum of the idler wave of the OPA. The autocorrelation width is 160 fs (assuming a sech^2 pulse shape), and the spectrum FWHM is 88 nm; these values give a time–bandwidth product of 0.58. The idler pulses from the OPA are 1.8 times the transform limit for a sech^2 pulse. The sharp features in the OPA idler spectrum are due to water-vapor absorption in air.

The autocorrelation signal at 2.75 μm is produced with a type-I phase-matched $LiIO_3$ ($\theta = 42°$) and is detected with an InGaAs detector, a beam chopper, and a lock-in amplifier combination. At full output power the FWHM is 160 fs (assuming a sech^2 pulse shape). Broadening effects from atmospheric water vapor require maintenance of a purged path between the OPA and the autocorrelator. Pulse broadening in the OPA crystal is a potential problem because of the group-velocity difference between the pump and the idler waves as they pass through a KTP twice,[30] but one can control this problem by reducing the crystal thickness.

An estimate of the power density in the OPA is obtained by comparison of the performance with different focusing lenses. With a beam radius of 1 mm at the lens, a lens of 15-cm focal length produces self-focusing at the focus. A 20-cm focal-length lens results in lower gain than is optimum but causes no beam distortion or self-focusing. This result indicates that the optimum peak power at the focus approaches 10^{12} W/cm^2. Damage to the KTP crystal does not occur if its surfaces are kept clean.

It is important to distinguish between difference-frequency mixing and optical parametric amplification. From the pump and the seed pulse energies at the KTP crystal (6 μJ and 2 nJ) and assuming perfect beam overlap, one calculates that the infrared pulse energy produced from difference-frequency mixing is $\sim$1 nJ at 2.75 μm (assuming 100% conversion efficiency), which is much less than the observed result of 500 nJ. The OPA

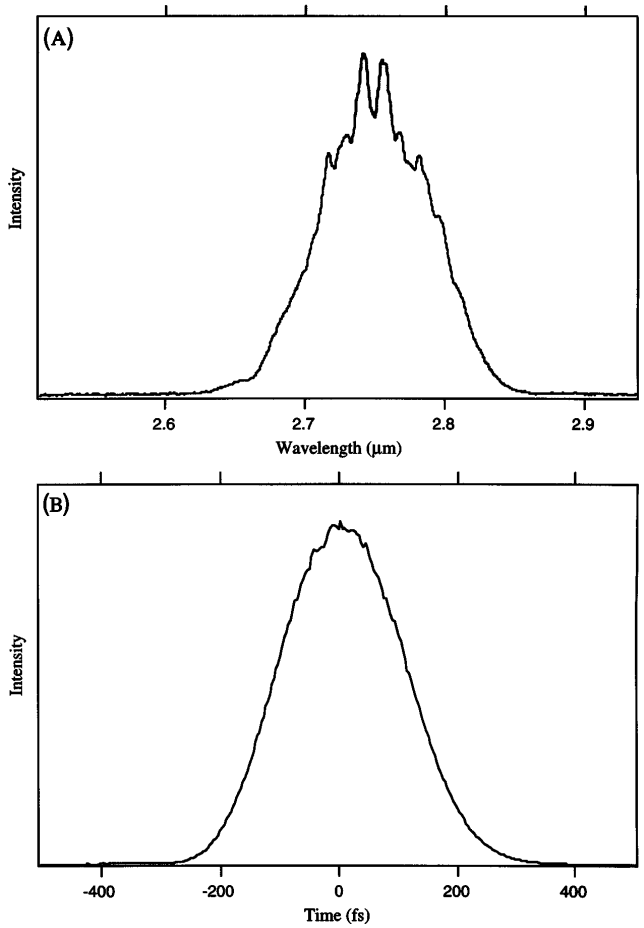

Fig. 8. (A) Spectrum of the OPA idler wave for a pump wavelength of 817 nm. The FWHM is 88 nm. The sharp features are due to absorption by water vapor. (B) Autocorrelation of the OPA idler wave. Assuming a sech^2 pulse shape, the FWHM is 160 fs. The pulses are 1.8 times the transform limit.

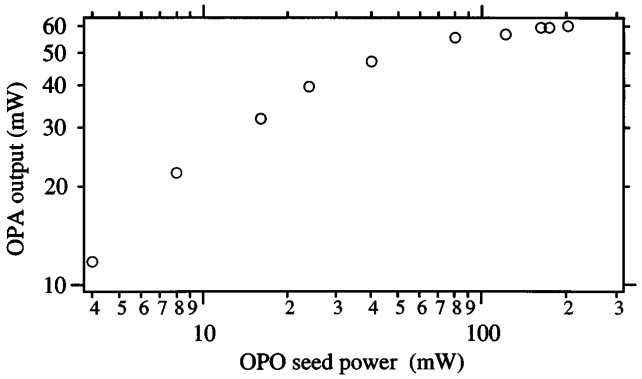

Fig. 9. Dependence of idler-wave output power of the OPA on the OPO seed power. For seeding powers greater than ~100 mW the OPA begins to saturate. The pump pulse energy is 4 μJ.

starts to saturate in energy for signal energies above ~1 nJ (~100 mW), as indicated by Fig. 9. The parametric amplification factor decreases from its small-signal limit of at least 2000 to the saturated value of 520.

6. CONCLUSION

We have demonstrated a high-repetition-rate (250-kHz) high-peak-power (≥3 MW), femtosecond infrared laser source that will make it possible to conduct nonlinear and pump–probe experiments in the chemically important 3-μm region. The system is capable of generating 106-fs pulses with 550 nJ of energy and is tunable from 2.5 to 2.9 μm. We have shown KTP to be robust and efficient for use in an OPA and that it operates at wavelengths longer than those accessible with the more widely used β-BaB_2O_4 and LiB_3O_5 crystals. The time resolution of the system has been shown to be fast enough to resolve dephasing dynamics of liquid-water molecules at room temperature.[34,35]

ACKNOWLEDGMENTS

This research was conducted at the Pacific Northwest Laboratory, a multiprogram national laboratory operated by Battelle Memorial Institute for the Department of Energy under contract DE-AC06-76LO 1830.

Address correspondence and reprint requests to G. Holtom.

REFERENCES

1. H. Graener, G. Seifert, and A. Laubereau, "New spectroscopy of water using tunable picosecond pulses in the infrared," Phys. Rev. Lett. **66,** 2092–2095 (1991).
2. A. Tokmakoff, D. Zimdars, B. Sauter, R. S. Francis, A. S. Kwok, and M. D. Fayer, "Vibrational photon echoes in a liquid and a glass: room temperature to 10 K," J. Chem. Phys. **101,** 1741–1744 (1994).
3. D. Zimdars, A. Tokmakoff, S. Chen, S. R. Greenfield, and M. D. Fayer, "Picosecond infrared vibrational photon echoes in a liquid and glass using a free electron laser," Phys. Rev. Lett. **70,** 2718–2721 (1993).
4. Herman Vanherzeele, "Picosecond laser system continuously tunable in the 0.6–4-μm range," Appl. Opt. **29,** 2246–2258 (1990).
5. H. M. van Driel and G. Mak, "Femtosecond pulses from the ultraviolet to the infrared: optical parametric processes in a new light," Can. J. Phys. **71,** 47–58 (1993).
6. R. Danielius, A. Piskarskas, A. Stabinis, G. P. Banfi, P. Di Trapani, and R. Righini, "Traveling-wave parametric generation of widely tunable, highly coherent femtosecond light pulses," J. Opt. Soc. Am. B **10,** 2222–2232 (1993).
7. G. P. Banfi, R. Danielius, A. Piskarskas, P. Di Trapani, P. Foggi, and R. Righini, "Femtosecond traveling-wave parametric generation with lithium triborate," Opt. Lett. **18,** 1633–1635 (1993).
8. R. Baumgartner and R. L. Byer, "Optical parametric amplification," IEEE J. Quantum Electron. **QE-15,** 432–444 (1979).
9. A. Tokmakoff, C. D. Marshall, and M. D. Fayer, "Optical parametric amplification of 1-kHz high-energy picosecond midinfrared pulses and application to infrared transient-grating experiments on diamond," J. Opt. Soc. Am. B **10,** 1785–1791 (1993).
10. W. Joosen, P. Agostini, G. Petite, J. P. Chambaret, and A. Antonetti, "Broadband femtosecond infrared parametric amplification in β-BaB_2O_4," Opt. Lett. **17,** 133–135 (1992).
11. R. Laenen, K. Wolfrum, A. Seilmeier, and A. Laubereau, "Parametric generation of femtosecond and picosecond pulses for spectroscopic applications," J. Opt. Soc. Am. B **10,** 2151–2160 (1993).
12. F. Seifert, V. Petrov, and F. Noack, "Sub-100-fs optical parametric generator pumped by a high-repetition-rate Ti:sapphire regenerative amplifier system," Opt. Lett. **19,** 837–839 (1994).
13. S. J. Bronsan and R. L. Byer, "Optical parametric oscillator threshold and linewidth studies," IEEE J. Quantum Electron. **QE-15,** 415–431 (1979).
14. J. M. Dudley, D. T. Reid, M. Ebrahimzadeh, and W. Sibbett, "Characteristics of a noncritically phase matched Ti:sapphire pumped femtosecond optical parametric oscillator," Opt. Commun. **104,** 419–430 (1994).
15. Q. Fu, G. Mak, and H. M. van Driel, "High-power, 62-fs infrared optical parametric oscillator synchronously pumped by a 76-MHz Ti:sapphire laser," Opt. Lett. **17,** 1006–1008 (1992).
16. P. E. Powers, C. L. Tang, and L. K. Cheng, "High-repetition-rate femtosecond optical parametric oscillator based on $CsTiOAsO_4$," Opt. Lett. **19,** 37–39 (1994).
17. P. E. Powers, S. Ramakrishna, C. L. Tang, and L. K. Cheng, "Optical parametric oscillation with $KTiOAsO_4$," Opt. Lett. **18,** 1171–1173 (1993).
18. P. E. Powers, R. J. Ellingson, W. S. Pelouch, and C. L. Tang, "Recent advances of the Ti:sapphire-pumped high-repetition-rate femtosecond optical parametric oscillator," J. Opt. Soc. Am. B **10,** 2162–2167 (1993).
19. W. R. Bosenberg and R. H. Jarman, "Type-II phase-matched $KNbO_3$ optical parametric oscillator," Opt. Lett. **18,** 1323–1325 (1993).
20. S. D. Butterworth, M. J. McCarthy, and D. C. Hanna, "Widely tunable synchronously pumped optical parametric oscillator," Opt. Lett. **18,** 1429–1431 (1993).
21. W. S. Pelouch, P. E. Powers, and C. L. Tang, "Ti:sapphire-pumped, high-repetition-rate femtosecond optical parametric oscillator," Opt. Lett. **17,** 1070–1072 (1992).
22. P. E. Powers, C. L. Tang, and L. K. Cheng, "High-repetition-rate femtosecond optical parametric oscillator using $RbTiOAsO_4$," Opt. Lett. **19,** 1439–1441 (1994).
23. Ch. Grässer, D. Wang, R. Beigang, and R. Wallenstein, "Singly resonant optical parametric oscillator of $KTiOPO_4$ synchronously pumped by the radiation of a continuous-wave mode-locked Nd:YLF laser," J. Opt. Soc. Am. B **10,** 2218–2221 (1993).
24. G. J. Hall, M. Ebrahimzadeh, A. Robertson, G. P. A. Malcolm, and A. I. Ferguson, "Synchronously pumped optical parametric oscillators using all-solid-state pump lasers," J. Opt. Soc. Am. B **10,** 2168–2179 (1993).
25. Gary Mak, Qiang Fu, and Henry M. van Driel, "Externally pumped high repetition rate femtosecond infrared optical parametric oscillator," Appl. Phys. Lett. **60,** 542–544 (1992).
26. M. J. McCarthy and D. C. Hanna, "All-solid-state synchro-

nously pumped optical parametric oscillator," J. Opt. Soc. Am. B **10,** 2180–2190 (1993).
27. J. A. Moon, "Characterization and modeling of a femtosecond optical parametric oscillator suitable for tunable pump–probe spectroscopy," IEEE J. Quantum Electron. **29,** 265–269 (1993).
28. D. C. Edelstein, E. S. Wachman, and C. L. Tang, "Broadly tunable high repetition rate femtosecond optical parametric oscillator," Appl. Phys. Lett. **54,** 1728–1730 (1989).
29. A. Robertson and A. I. Ferguson, "Synchronously pumped all-solid-state lithium triborate optical parametric oscillator in a ring configuration," Opt. Lett. **19,** 117–119 (1994).
30. A. Nebel, C. Fallnich, R. Beigang, and R. Wallenstein, "Noncritically phase-matched continuous-wave mode-locked singly resonant optical parametric oscillator synchronously pumped by a Ti:sapphire laser," J. Opt. Soc. Am. B **10,** 2195–2200 (1993).
31. A. Agnesi, G. C. Reali, V. Kubecek, S. Kumazaki, Y. Takagi, and K. Yoshihara, "β-Barium borate and lithium triborate picosecond parametric oscillators pumped by a frequency-tripled passive negative-feedback mode-locked Nd:YAG laser," J. Opt. Soc. Am. B **10,** 2211–2217 (1993).
32. K. Kato, "Parametric oscillation at 3.2 μm in KTP pumped at 1.064 μm," IEEE J. Quantum Electron. **27,** 1137–1140 (1991).
33. G. R. Holtom, R. A. Crowell, and X. S. Xie, "Noncritically phase-matched femtosecond optical parametric oscillator near 3 microns," in *Advanced Solid-State Lasers*, T. Y. Fan and B. H. T. Chai, eds., Vol. 20 of OSA Proceedings Series (Optical Society of America, Washington, D.C., 1994), pp. 407–409.
34. R. A. Crowell, G. R. Holtom, and X. S. Xie, "Liquid water dynamics probed by femtosecond infrared spectroscopy," in *Ultrafast Phenomena IX*, P. F. Barbara, W. H. Knox, G. A. Mourou, and A. H. Zewail, eds. (Springer-Verlag, New York, 1994), pp. 156–158.
35. R. A. Crowell, G. R. Holtom, and X. S. Xie, "The infrared free induction decay of liquid water molecules," J. Phys. Chem. **99,** 1840–1842 (1995).
36. L. F. Mollenauer, "Color center lasers," in *Laser Handbook*, M. L. Stitch and M. Bass, eds. (North-Holland, Amsterdam, 1985), Vol. 4, pp. 143–228.
37. T. Dahinten, K. L. Vodopyanov, U. Plöderender, A. Seilmeier, K. R. Allakhverdiev, and Z. A. Ibragimov, "Infrared pulses of 1 picosecond duration tunable between 4 μm and 18 μm," IEEE J. Quantum Electron. **29,** 2245–2250 (1993).
38. E. S. Wachman, D. C. Edelstein, and C. L. Tang, "Continuous-wave mode-locked and dispersion-compensated femtosecond optical parametric oscillator," Opt. Lett. **15,** 136–139 (1990).
39. David A. Roberts, "Simplified characterization of uniaxial and biaxial nonlinear optical crystals: a plea for standardization of nomenclature and conventions," IEEE J. Quantum Electron. **28,** 2057–2074 (1992).
40. J. Q. Yao and T. S. Fahlen, "Calculations of optimum phase match parameters for the biaxial crystal $KTiOPO_4$," J. Appl. Phys. **55,** 65–68 (1984).
41. D. W. Anthon and D. C. Crowder, "Wavelength dependent phase matching in KTP," Appl. Opt. **27,** 2650–2652 (1988).
42. H. Vanherzeele, J. D. Bierlein, and F. C. Zumsteg, "Index of refraction measurements and parametric generation in hydrothermally grown $KTiOPO_4$," Appl. Opt. **27,** 3314–3316 (1988).
43. E. C. Cheung and J. M. Liu, "Theory of a synchronously pumped optical parametric oscillator in steady-state operation," J. Opt. Soc. Am. B **7,** 1385–1401 (1990); E. C. Cheung and J. M. Liu, "Efficient generation of ultrashort, wavelength-tunable infrared pulses," J. Opt. Soc. Am. B **8,** 1491–1506 (1991).
44. A. E. Siegman, *Lasers* (University Science, Mill Valley, Calif., 1986), pp. 581–625.
45. G. D. Boyd and D. A. Kleinman, "Parametric interaction of focused Gaussian light beams," J. Appl. Phys. **39,** 3597–3639 (1968).
46. J.-K. Rhee, T. S. Sosnowski, T. B. Norris, J. A. Arns, and W. S. Colburn, "Chirped-pulse amplification of 85-fs pulses at 250 kHz with third-order dispersion compensation by use of holographic transmission gratings," Opt. Lett. **19,** 1550–1552 (1994).